Density Functional Study of the Primary Photoprocesses of Manganese Pentacarbonyl Chloride ($MnCl(CO)_5$)

Maikel P. Wilms,[†] Evert Jan Baerends,*[,†] Angela Rosa,[‡] and Derk J. Stufkens[§]

Afdeling Theoretische Chemie, Vrije Universiteit, De Boelelaan 1083, 1081 HV, Amsterdam, The Netherlands, Dipartimento di Chimica, Universitá della Basilicata, Via N. Sauro, 85, 85100 Potenza, Italy, and Anorganisch Chemisch Laboratorium, J. H. van't Hoff Research Insitute, Universteit van Amsterdam, Nieuwe Achtergracht 166, 1018 WV, Amsterdam, The Netherlands

Received June 10, 1996[⊗]

Density functional calculations have been performed on the ground and excited states of $MnCl(CO)_5$ in order to explain the photochemistry of $MX(CO)_5$ complexes (M = Mn, Re; X = Cl, Br, I). As found earlier for $Mn_2(CO)_{10}$ (*Inorg. Chem.* **1996**, *35*, 2886), the e_g-type unoccupied 3d orbitals in the pseudooctahedral environment are located rather high in the virtual orbital spectrum, and the corresponding ligand-field (LF) excitations are more than 1 eV above the lowest excitations. Potential energy curves (PECs) nevertheless show that the lowest excited states, which involve transitions to the Mn−Cl σ^* orbital at equilibrium geometry, are dissociative for axial and equatorial CO loss. The mechanism is again, as in $Mn_2(CO)_{10}$, a strongly avoided crossing of the lowest excited state ($a^{1,3}E$) with the higher dissociative LF states (different ones for CO_{ax} and CO_{eq} dissociation) which rapidly descend upon Mn−CO bond lengthening. In spite of the lowest excitation being to the Mn−Cl σ^*-orbital, Mn−Cl homolysis cannot occur out of the lowest excited state. The photochemical behavior of $Mn_2(CO)_{10}$, $MnH(CO)_5$, and $MnCl(CO)_5$ is compared. The mechanisms of CO loss are found to be very similar, but there is a large difference with respect to the breaking of the σ bond (Mn−Mn, Mn−H, or Mn−Cl). Only in the case of $Mn_2(CO)_{10}$, the lowest broad absorption band contains the $\sigma \rightarrow \sigma^*$ excitation and leads to σ bond breaking.

1. Introduction

Detailed insight into photochemical pathways of organometallic compounds is rapidly accumulating due to the use of sophisticated equipment for the detection of excited states and reactive intermediates.[1] At the same time, the advances in quantum mechanical methods and computer technology have made feasible extensive calculations on both ground and excited states of simple organometallic complexes. Especially the calculation of potential energy curves (PECs) has proven to be very valuable in describing the photochemistry of transition metal complexes[2] (see also refs 3−5).

In this paper we will focus on the photochemistry of $MnCl(CO)_5$. Many studies on the photochemistry of metal pentacarbonyl halides show that CO loss is the primary photoprocess.[6,7] From these studies it is known that in $MnCl(CO)_5$ only the Mn−CO bond is photolytically cleaved and that no Mn−Cl bond homolysis occurs. In the absence of coordinating species, the photochemistry yields the halide-linked dimer $Mn_2(CO)_8Cl_2$, while in the presence of coordinating species the *cis* substituted product is formed. It is somewhat surprising that the photosubstitution reaction is highly stereospecific, yielding only the *cis* isomer. Within the usual ligand-field picture (cf. Wrighton *et al.*[7]), one would expect the LUMO to be the metal d_{z^2} orbital, which is assumed to have more antibonding interaction with the axial CO than with the chlorine. Irradiation into the lowest ligand-field (LF) band increases the population of this d_{z^2} orbital and would be expected to result in loss of CO *trans* to chlorine. The LF view thus predicts a different primary photoproduct than experiment suggests. This inconsistency can be resolved if one assumes that indeed an intermediate resulting from axial CO loss occurs (a square pyramid with Cl in the apical position), but that this intermediate is susceptible to an excited state rearrangement to a square pyramid with Cl in basal position. Subsequent addition of a coordinating ligand then results in a *cis* substituted product. The possible rearrangement pathways of the $MnCl(CO)_4$ intermediate have received considerable attention recently (cf. Pierloot *et al.*[4] and Matsubara *et al.*[8c]). One expects in the LF picture to have the other e_g-type orbital ($d_{x^2-y^2}$) at higher energy than the d_{z^2} orbital, because Cl is a weaker σ donor than CO. Occupation

[†] Vrije Universiteit.
[‡] Università della Basilicata.
[§] Universiteit van Amsterdam.
[⊗] Abstract published in *Advance ACS Abstracts,* February 1, 1997.

(1) See, for some recent examples: (a) Nieuwenhuis, H. A.; Stufkens, D. J.; McNicholl, R.-A.; Al-Obaidi, A. H.; Coates, G. C.; Bell, S. E. J.; McGarvey, J. J.; Westwell, J.; George, M. W.; Turner, J. J. *J. Am. Chem. Soc.* **1995**, *117*, 5579. (b) Kim, S. K.; Pederso, S.; Zewail, A. H. *Chem. Phys. Lett.* **1995**, *233*, 500. (c) Schoonover, J. R.; Strouse, G. F.; Dyer, R. B.; Bates, W. D.; Chen, P.; Meyer, T. J. *Inorg. Chem.* **1996**, *35*, 273.

(2) (a) Daniel, C.; Bénard, M.; Dedieu, A.; Wiest, R.; Veillard, A. *J. Phys. Chem.* **1984**, *88*, 4805. (b) Daniel, C.; Hyla-Krypsin, I.; Demuynck, J.; Veillard, A. *Nouv. J. Chim.* **1985**, *9*, 581. (c) Veillard, A.; Strich, A. *J. Am. Chem. Soc.* **1988**, *110*, 3793. (d) Daniel, C. *Coordination Chemistry Reviews: Proceedings of the 8th International Symposium on the Photochemistry and Photophysics of Coordination Compounds*; Elsevier Science Publishers B. V.: Amsterdam, 1990; Vol. 97, p 141. (e) Daniel, C. *J. Phys. Chem.* **1991**, *95*, 2394. (f) Röhmer, M. M.; Veillard, A. *New. J. Chem.* **1991**, *15*, 795. (g) Daniel, C. *J. Am. Chem. Soc.* **1992**, *114*, 1625. (h) Finger, K.; Daniel, C. *J. Chem. Soc., Chem. Commun.* **1995**, 1427. (i) Finger, K.; Daniel, C. *J. Am. Chem. Soc.* **1995**, *117*, 12322.

(3) (a) Rosa, A.; Ricciardi, G; Baerends, E. J.; Stufkens, D. J. *Inorg. Chem.* **1995**, *34*, 3425. (b) Rosa, A.; Ricciardi, G; Baerends, E. J.; Stufkens, D. J. *Inorg. Chem.* **1996**, *35*, 2886.

(4) Pierloot, K.; Hoet, P.; Vanquickenborne, L. G. *J. Chem. Soc., Dalton Trans.* **1991**, 2363.

(5) Pierloot, K.; Hoet, P.; Vanquickenborne, L. G. *Inorg. Chim. Acta* **1991**, *184*, 147.

(6) McHugh, T. M.; Rest, A. J.; Taylor, D. J. *J. Chem. Soc., Dalton Trans.* **1980**, 1803.

(7) Wrighton, M. S.; Morse, D. L.; Gray, H. B.; Otteson, D. K. *J. Am. Chem. Soc.***1976**, *98*, 1111.

S0020-1669(96)00688-X CCC: $14.00

of this orbital would lead to equatorial CO loss. In view of the dramatic increase of the quantum yield when going to higher excitation energies and the temperature dependence of both the quantum yield and the lifetime, Wrighton *et al*.[7] concluded that indeed such a higher lying photoactive excited state with $d_{x^2-y^2}$ character is present. These results were supported by the calculations by Pierloot *et al*.[4,5]

This picture of the photochemistry of $MnCl(CO)_5$ is based on the accepted paradigm of photolabilization of metal−carbonyl bonds by ligand field excitation. We have, however, recently found[3b] in the case of $Mn_2(CO)_{10}$ that this picture may require considerable adjustment and refinement. The calculation of PECs for CO dissociation and Mn−Mn bond breaking, and an analysis of the electronic structure of the ground and excited states,[3a] revealed that among the lowest excited states the $^{1,3}E_1$ ($d_\pi \rightarrow \sigma^*$) state is $Mn-CO_{ax}$ dissociative, although it is not Mn−CO antibonding and cannot unequivocally be assigned as a LF excited state. There are, however, strongly Mn−CO antibonding $3d-e_g$-type orbitals located at fairly high energy in the virtual orbital spectrum. Excitations to such orbitals lead to LF excited states with strongly dissociative PECs. These PECs rapidly become lower in energy with increasing Mn−CO distance and cross the low-lying excited $^{1,3}E_1$ states. In this way these low-lying excited states become Mn−CO dissociative, although the avoided crossing may lead to a barrier. This picture is at variance with the LF picture indicated above for the photochemistry of $MnCl(CO)_5$, which assumes a population of dissociative LF states directly upon low-energy irradiation.

The $MnCl(CO)_5$ system is well-suited for further investigation of this issue, since it offers the additional possibility of photochemical cleavage of a metal−ligand σ bond and may thus be compared to other well-studied $Mn(CO)_5L$ systems such as $MnH(CO)_5$ and $Mn_2(CO)_{10}$. In $Mn_2(CO)_{10}$ the Mn−Mn bond is broken with approximately equal probability as the Mn−CO bond upon irradiation into the lowest absorption band. This may be attributed[3b] to transition to the low-lying $^3B_2$, of Mn−Mn $\sigma \rightarrow \sigma^*$ character, which is nearly degenerate with the Mn−CO dissociative $^{1,3}E_1$ states. However, the Mn−H bond of $MnH(CO)_5$ is broken only upon high-energy irradiation, with relatively low quantum yield, although Mn−CO dissociation occurs as in $Mn_2(CO)_{10}$ from the low-lying excited states. Veillard *et al*. explained the wavelength dependent photochemistry of $MnH(CO)_5$ by calculating CASSCF/CCI correlation diagrams for both axial CO and H loss.[8] It was found that the lowest excited state is dissociative with respect to axial CO, whereas higher excited states are dissociative with respect to both axial CO and hydrogen. This conclusion was confirmed by full calculation of the PECs by Daniel,[2g] although these PECs demonstrated that the picture is complicated by several avoided crossings, resulting in small barriers.

In order to elucidate the photochemistry of $MnCl(CO)_5$ and study the similarities and differences with other $Mn(CO)_5$ derivatives, we have calculated PECs for both axial and equatorial CO loss and for Cl homolysis. The results are discussed in section 4 and indicate that both axial and equatorial CO loss can occur, but only due to a (strongly) avoided crossing with the lowest excited state by a dissociative LF excited state, which is high-lying at the equilibrium geometry but descends rapidly upon Mn−CO bond lengthening. Mn−Cl bond breaking does not occur. The CO loss mechanisms of $MnH(CO)_5$, $MnCl(CO)_5$, and $Mn_2(CO)_{10}$ are compared as well as the breaking of the σ bond (Mn−Mn, Mn−H, Mn−Cl). The first are very similar, the latter are very different in these compounds.

Before dealing with the photochemistry of the title compound, we first elucidate in section 3 the electronic structure of $MnCl(CO)_5$, which is a prerequisite for understanding the photochemistry. The electronic structure of manganese pentacarbonyl halides has been the subject of many theoretical,[9,10] ultraviolet photoelectron spectroscopic (UPS),[11−16] and UV−vis spectroscopic studies.[7,17−19] For the present purpose in particular the molecular orbital structure and the excitation spectrum are relevant and will be discussed in section 3. Section 4 discusses the photochemistry and section 5 contains the Conclusions, in particular with respect to the role of LF excited states in the photodissociation process.

2. Computational Details

All calculations have been performed using the Amsterdam density functional program package ADF.[23] The computational scheme is characterized by the use of a density-fitting procedure to obtain accurate Coulomb and exchange potentials in each self-consistent field (SCF) cycle, by the accurate and efficient numerical integration[24] of the Hamiltonian matrix elements and the possibility to freeze core orbitals. We used an uncontracted double-ζ STO basis set with one polarization function for all atoms, except for the manganese orbitals for which a triple-ζ 3d,4s basis with one 4p function was used. The 1s oxygen and carbon cores were kept frozen as well as the 1s−2p cores for manganese and chlorine.

The ground and excited state energies included Becke's[25] nonlocal corrections to the local expression[26] of the exchange energy and Perdew's[27] nonlocal corrections to the local expression (Vosko−Wilk−Nusair[28] parametrization of electron gas data) for the correlation energy.

(8) (a) Daniel, C.; Veillard, A *Nouv. J. Chim.* **1986**, *10*, 83. (b) Veillard, A.; Daniel, C.; Strich, A. *Pure Appl. Chem.* **1988**, *60* (2), 215. (c) Matsubara, T.; Daniel, C.; Veillard, A. *Organometallics* **1994**, *13*, 4905.

(9) Fenske, R. F.; DeKock, R. L. *Inorg. Chem.* **1970**, *9*, 1053.
(10) Davy, R. D.; Hall, M. B. *Inorg. Chem.* **1989**, *28*, 3524.
(11) Evans, S.; Green, J. C.; Green, M. L. H.; Orchard, A. F.; Turner, D. W. *Discuss. Faraday Soc*. **1969**, *47*, 112.
(12) Lichtenberger, D. L.; Sarapu, A. C.; Fenske, R. F. *Inorg. Chem.* **1973**, *12*, 702.
(13) Caesar, G. P.; Milazzo, P.; Cihonski, J. L.; Levenson, R. A. *Inorg. Chem.* **1974**, *13*, 3035.
(14) Higginson, B. R.; Lloyd, D. R.; Evans, S.; Orchard, A. F. *J. Chem. Soc., Faraday Trans. 2* **1975**, *71*, 1913.
(15) Jolly, W. L. *J. Phys. Chem.* **1983**, *87*, 26.
(16) DeKock, R. L. Ultraviolet Photoelectron Spectroscopy of Inorganic Molecules. In *Electron Spectroscopy Theory, Techniques and Applications*; Brundle, C. R., Baker, A. D., Eds.; Academic Press: New York, 1977; Vol. 1.
(17) Gray, H. B.; Billig, E.; Wojcicki, A.; Farona, M. *Can. J. Chem*. **1963,** *41*, 1281.
(18) Blackney, G. B.; Allen, W. F. *Inorg. Chem*. **1971**, *10*, 2763.
(19) McLean, R. A. N. *J. Chem. Soc., Dalton Trans.* **1974**, 1568.
(20) Spiess, H. W.; Sheline, R. K. *J. Chem. Phys.* **1971**, *54*, 1099.
(21) (a) Hillier, I. H.; Guest, M. F.; Higginson, B. R.; Lloyd, D. R. *Mol. Phys*. **1974**, *27*, 215. (b) Evans, S.; Guest, M. F.; Hillier, I. H.; Orchard, A. F. *J. Chem. Soc., Faraday Trans. 2* **1974**, *70*, 417. (c) Coutière, M. M.; Demuynck, J.; Veillard, A. *Theor. Chim. Acta* **1972**, *27*, 281. (d) Röhmer, M. M.; Veillard, A. *J. Chem. Soc., Chem. Commun.* **1973**, 250.
(22) Vliek, R. M. E.; Zandstra, P. J. *Chem. Phys. Lett*. **1975**, *31*, 487.
(23) (a) Baerends, E. J.; Ellis, D. E.; Ros, P. *Chem. Phys*. **1973**, *2*, 52. (b) Baerends, E. J.; Ros, P. *Int. J. Quantum Chem.* **1978**, *S12*, 169.
(24) (a) Boerrigter, P. M.; Te Velde, G.; Baerends, E. J. *Int. J. Quantum Chem.* **1988**, *33*, 87. (b) Te Velde, G.; Baerends, E. J. *J. Comput. Phys.* **1992**, *99*, 84.
(25) (a) Becke, A. D. *J. Chem. Phys.* **1986**, *84*, 4524. (b) Becke, A. D. *Phys. Rev*. **1988**, *A38*, 3098.
(26) Parr, R. G.; Yang, W. *Density Functional Theory of Atoms and Molecules*; Oxford University Press: New York, 1989.
(27) (a) Perdew, J. P. *Phys. Rev*. **1986**, *B33*, 8822. (b) Perdew, J. P. *Phys. Rev*. **1986**, *B34*, 7406.
(28) Vosko, S. H.; Wilk, L.; Nusair, M. J. *Can. J. Phys*. **1980**, *58*, 1200.

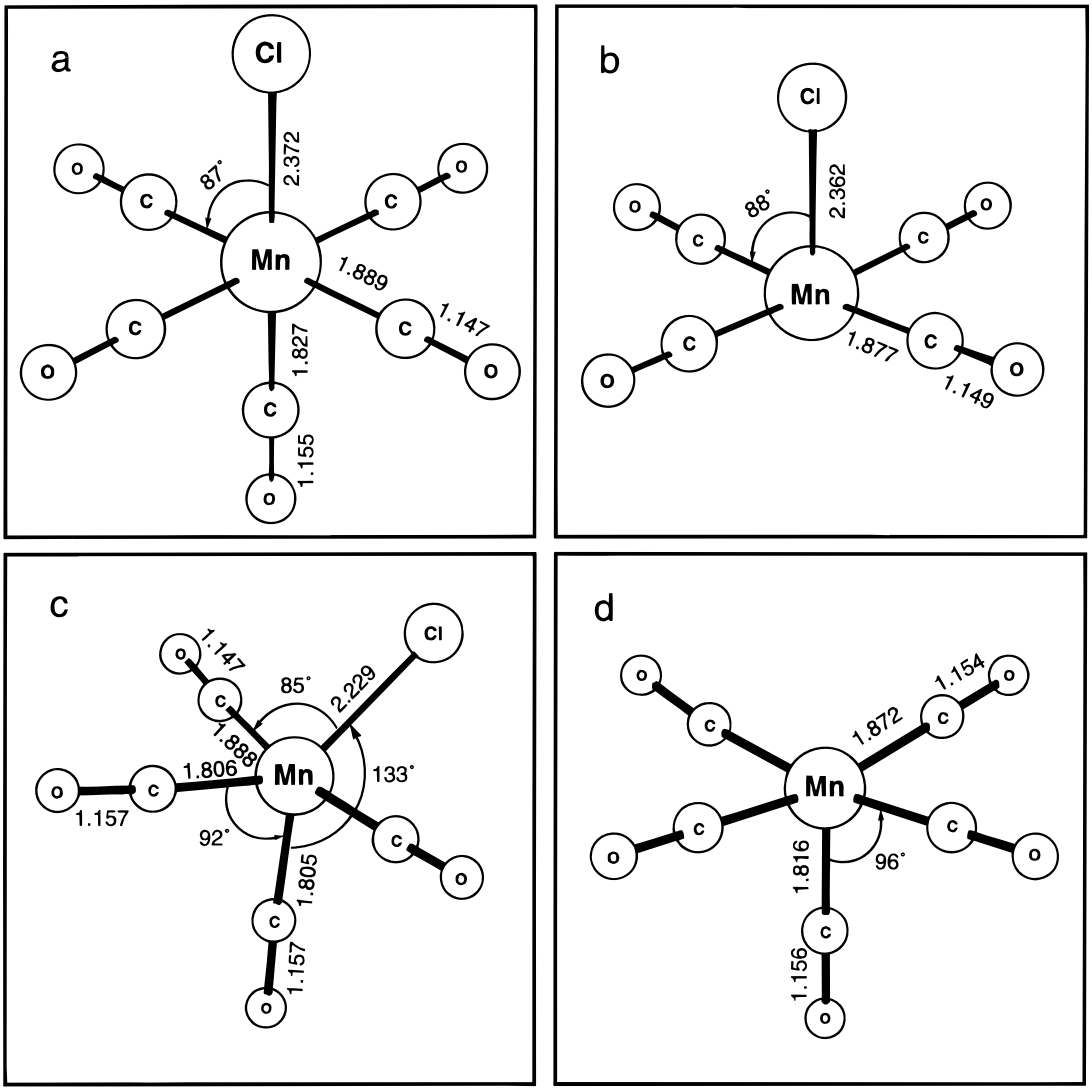

Figure 1. Geometry of (a) $MnCl(CO)_5$, (b) apical $MnCl(CO)_4$, (c) basal $MnCl(CO)_4$, and (d) $Mn(CO)_5$ (bond distances in angstroms).

The original proof of the Hohenberg−Kohn theorem[29] is only valid for the ground state of a system, and while it has been extended to the lowest state of any given symmetry,[30] this still does not suffice for a full description of the photochemical properties of molecules. However, the approximate method introduced by Ziegler *et al*.[31] for the calculation of excited states has been used with good results for both atomic[32] and molecular systems.[33] It has recently been applied successfully for the calculation of a two-dimensional potential energy surface for the photodissociation of H_2O in its first excited state[34] and compared to *ab initio* calculations and experiment. The photochemistry of $Mn_2(CO)_{10}$ has also been investigated with this method.[3b] In its simplest form, the method of ref 31 incorporates the relaxation effects in the excited state by an SCF calculation on a single-determinantal state, representing one of the multiplet states. Although this method yields results which are in keeping with experiment, it is only formally justified for the lowest state of each symmetry. Therefore, we will avoid drawing conclusions from the quantitative results of calculations on higher states. We feel, however, justified to use these results qualitatively.

The geometry of $MnCl(CO)_5$ as specified in Figure 1a was taken from an earlier density functional theory (DFT) study on this molecule.[35] In order to be able to compare the dissociation with experiment, geometry optimizations have been performed for the $Mn(CO)_5$ and $MnCl(CO)_4$ photoproducts using gradient techniques.[36] The results are shown in Figure 1b−d. The photoproducts resulting from axial CO or Cl loss have geometries which have only relaxed a little. $MnCl(CO)_4$ with an equatorial vacancy, however, shows considerable relaxation. In order to keep calculations tractable, geometry optimizations were not carried out at all points on the PEC. However, in order to assess at which point during the dissociation relaxation can come into play, we have optimized the geometry of the $MnCl(CO)_5$ fragment at a fixed distance $Mn-CO_{eq}$ of 2.3 Å, at which point the PECs approach their asymptotic shape (see below). The optimized geometry at this point differed only slightly from the

(29) Hohenberg, P.; Kohn, W. *Phys. Rev.* **1964**, *B136*, 864.
(30) (a) Gross, E. K. U.; Oliveira, L. N.; Kohn, W. *Phys. Rev.* **1988**, *A37*, 2805, 2809, 2821. (b) Gunnarson, O.; Lundqvist, B. I. *Phys. Rev.* **1976**, *B13*, 4274.
(31) Ziegler, T.; Rauk, A.; Baerends, E. J. *Theor. Chim. Acta* **1977**, *43*, 261.
(32) (a) von Barth, U. *Phys. Rev.* **1979**, *A20*, 1693. (b) Lannoo, M.; Baraff, G. A.; Schlüter, M. *Phys. Rev.* **1981**, *B24*, 943.
(33) (a) Daul, C.; Baerends, E. J.; Vernooijs, P. *Inorg. Chem.* **1994**, *33*, 3543. (b) Ziegler, T.; Tschinke, V.; Becke, A. *J. Am. Chem. Soc.* **1987**, *109*, 1351. (c) Ziegler, T.; Tschinke, V.; Ursenbach, C. *J. Am. Chem. Soc.* **1987**, *109*, 4825. (d) Ziegler, T.; Tschinke, V.; Becke, A. *Polyhedron* **1987**, *6*, 685. (e) Ziegler, T.; Tschinke, V.; Versluis, L.; Baerends, E. J.; Ravenek, W. *Polyhedron* **1988**, *7*, 1625.
(34) Doublet, M. L.; Kroes, G. J.; Baerends, E. J.; Rosa, A. *J. Chem. Phys.* **1995**, *103*, 2538.
(35) van Eis, M. Internal report; Free University: Amsterdam, 1995.
(36) Versluis, L.; Ziegler, T. *J. Chem. Phys.* **1988**, *88*, 322.

Table 1. Orbital Energies and Percent Composition[a] (Based on Mulliken Population Analysis per MO) of the Lowest Unoccupied and Highest Occupied $MnCl(CO)_5$ Orbitals in Terms of Mn, Cl, CO_{ax}, and CO_{eq} Fragments

			percent composn				OP[b]		
orbital	orbital character	ϵ (eV)	Mn	Cl	CO_{ax}	CO_{eq}	Mn−Cl	Mn−CO_{ax}	Mn−CO_{eq}
				Unoccupied Orbitals					
16e	CO π^*	−1.944	2 ($d_{xz/yz}$)	1 (p_z)	37 ($2\pi^*$)	59 ($2\pi^*$)		0.02	−0.04
15e	"t_{2g}"	−2.785	22 ($d_{xz/yz}$)		42 ($2\pi^*$)	35 ($2\pi^*$)		−0.04	−0.05
$23a_1$	"e_g": d_{z^2} $\sigma^{*\prime}$	−2.796	39 (d_{z^2})	2 (p_z)	16 (5σ)	41 (34 $2\pi^*$, 7 5σ)	−0.01	−0.16	0.03
$8b_1$	CO π^*	−2.796	11 ($d_{x^2-y^2}$)			88 (80 $2\pi^*$, 8 $2\pi^*$)			−0.03
$3b_2$	"t_{2g}"	−2.983	31 (d_{xy})			69 ($2\pi^*$)			−0.11
$7b_1$	"e_g": $d_{x^2-y^2}$ $\sigma^{*\prime}$	−2.994	49 ($d_{x^2-y^2}$)			50 (31 5σ, 19 $2\pi^*$)			−0.14
14e	CO π^*	−3.197	5 ($d_{xz/yz}$)		6 ($2\pi^*$)	89 ($2\pi^*$)		0.01	−0.02
$22a_1$	(Mn−Cl) σ^*	−3.786	26 (20 d_{z^2}, 6 p_z)	20 (p_z)		55 ($2\pi^*$)	−0.08	−0.02	0.06
				Occupied Orbitals					
13e	Cl p_π − d_π	−6.447	18 ($d_{xz/yz}$)	74 ($p_{x/y}$)	3 ($2\pi^*$)	3 (5σ)	−0.02	0.01	−0.01
$2b_2$	"t_{2g}"	−8.010	68 (d_{xy})			32 ($2\pi^*$)			0.05
12e	"t_{2g}" d_π + Cl p_π	−8.030	54 ($d_{xz/yz}$)	22 ($p_{x/y}$)	8 ($2\pi^*$)	15 ($2\pi^*$)	0.03	0.01	0.02
$21a_1$	Cl p_σ	−8.386	18 (10 d_{z^2}, 8 p_z)	72 (p_z)	3 (5σ)	7 ($2\pi^*$)	0.06		
11e	CO 5σ	−11.409	6 ($p_{x/y}$)	1 ($p_{x/y}$)	13 ($2\pi^*$)	78 (65 5σ, 13 $2\pi^*$)		0.04	−0.01
$20a_1$	CO 5σ	−11.982	22 (d_{z^2})	1 (p_z)	47 (5σ)	28 ($2\pi^*$)		0.07	−0.01

[a] The major contribution is reported between parentheses; if there are several contributions of more than 5%, these are made explicit. [b] The Mulliken overlap populations are per orbital, based on a norm 1 of the orbital, i.e., an orbital occupation of 1 electron for occupied and virtual orbitals alike.

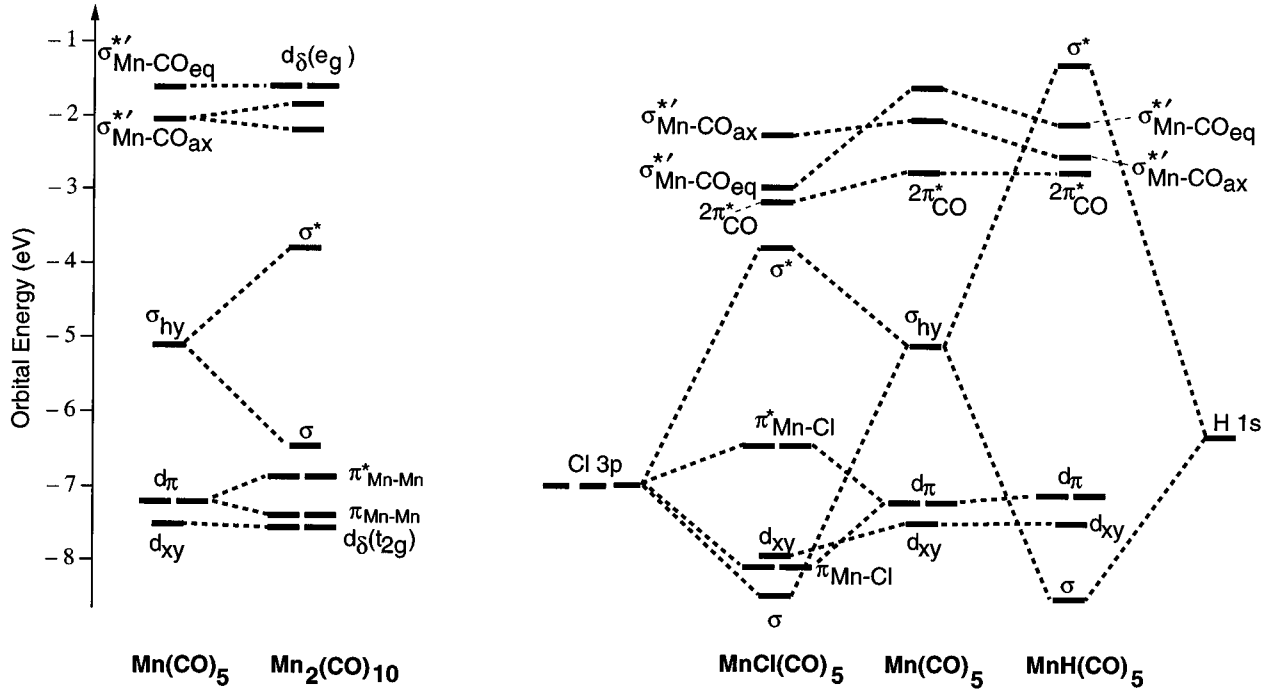

Figure 2. Orbital interaction diagrams for the formation of $Mn(CO)_5L$, where L = $Mn(CO)_5$, Cl, or H. The Cl 3p is not at the atomic level but is positioned so as to correctly suggest the composition of the orbitals.

"frozen" geometry. Furthermore femtosecond resolved experiments showed that the Mn−CO dissociation in $Mn_2(CO)_{10}$ occurs at a time scale of 20 fs.[1b] Since we find similar dissociative PECs as in $Mn_2(CO)_{10}$, the photodissociation process may be similar and thus much faster than the vibrations, which occur on the picosecond time scale. Therefore, it is not obvious that full geometry optimization along a Mn−CO dissociation coordinate would be justified, and we choose to calculate the PECs using a frozen geometry of the photodissociation fragments.

3. Electronic Structure

Ground State Electronic Structure. In order to better understand the photochemical behavior of $MnCl(CO)_5$, it is first of all necessary to know the characters of the highest occupied and lowest unoccupied molecular orbitals. These characters as well as the orbital energies are presented in Table 1. An orbital interaction diagram for the formation of $MnCl(CO)_5$ out of $Mn(CO)_5$ and Cl is shown in Figure 2.

The relevant occupied orbitals of $Mn(CO)_5$ are the fully occupied d_{xy} and the E pair of $d_{xz/yz}$ or d_π orbitals, which together correspond to the t_{2g} orbitals in O_h symmetry, and the singly occupied σ_{hy} orbital, which is a $3d_{z^2}$−$4p_z$−$2\pi^*_\perp$ hybrid, with its lobe directed toward the vacancy (the $2\pi^*_\perp$ denotes an a_1 combination of $2\pi^*$ orbitals of the equatorial CO's that are perpendicular to the equatorial plane). We refer to ref 3a for a detailed explanation of the orbital structure of $Mn(CO)_5$. In particular, it has been stressed that in $Mn(CO)_5$ one does not have a simple e_g-type (mostly $3d_{z^2}$) LUMO, but due to mixing with the $4p_z$ of Mn and the $2\pi^*_\perp$ of the equatorial CO's, there are two a_1 orbitals with considerable d_{z^2} character. The lowest one, the present σ_{hy} orbital ($10a_1$ in ref 3a) has little axial CO

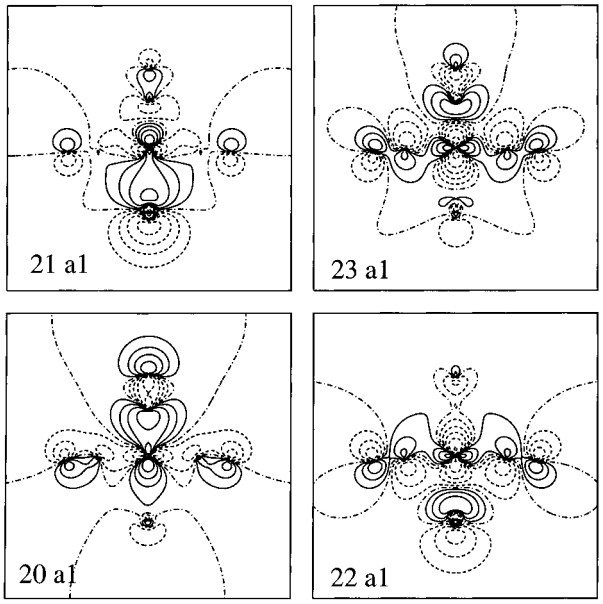

Figure 3. Contour plot of the $20a_1$, $21a_1$, $22a_1$, and $23a_1$ orbitals in the *xz*-plane. Contours values are ±0.5, ±0.2, ±0.1, ±0.05, ±0.02, and 0 $(e/bohr^3)^{1/2}$.

5σ character, and this orbital completely lacks the expected antibonding with the CO 5σ. On the other hand, the higher one ($11a_1$ in ref 3a), which is at considerably higher energy, lying within the CO π^* manifold, has considerable antibonding with the axial CO (it is denoted $\sigma^{*\prime}(Mn-CO_{ax})$ in Figure 2). Excitation to this latter orbital leads to strongly $Mn-CO_{ax}$ dissociative states. Due to the large amplitude of the $Mn(CO)_5$ σ_{hy} toward the vacant coordination site, interaction with a coordinating ligand is mostly through this orbital. In $Mn_2(CO)_{10}$ this leads to symmetrical σ and σ^* orbitals (the Mn−Mn bonding and antibonding combinations of the higher lying $\sigma^{*\prime}$-$(Mn-CO_{ax})$ do not split much due to their much lower amplitude at the vacant site). In the case of $MnCl(CO)_5$ a bonding σ orbital is formed with Cl p_σ (the $21a_1$; see Table 1) with predominantly Cl character, and an Mn−Cl σ antibonding orbital with mostly $Mn(CO)_5$ character, the $22a_1$ LUMO of $MnCl(CO)_5$. We will denote this orbital as $\sigma^*(Mn-Cl)$, or just σ^*. The high-lying $\sigma^{*\prime}(Mn-CO_{ax})$ of $Mn(CO)_5$ is practically unperturbed by the bonding with Cl, and it is found as the $23a_1$ orbital of $MnCl(CO)_5$. It is still about 1 eV above the $\sigma^*(Mn-Cl)$. Note that we differentiate between σ antibonding between Mn and L, denoted by σ^*, and σ antibonding between Mn and CO_{ax}, denoted by an additional prime, $\sigma^{*\prime}$. The situation is somewhat analogous to having two axial hybrids on Mn, one leading to (anti)bonding with axial CO, the other one with the other axial ligand L. The orbital plots in Figure 3 demonstrate the Mn−Cl bonding and antibonding characters of $21a_1$ and $22a_1$, respectively, and the Mn−CO bonding and antibonding character of the $20a_1$ and $23a_1$ (not $22a_1$!), respectively.

The description of the remaining occupied and unoccupied orbitals is straightforward. In the unoccupied spectrum we have fairly close to the strongly $Mn-CO_{ax}$ antibonding $\sigma^{*\prime}$ orbital ($23a_1$) the strongly $Mn-CO_{eq}$ σ antibonding $7b_1$ orbital derived from the $d_{x^2-y^2}$ component of the e_g-orbitals. We will also denote the $Mn-CO_{eq}$ σ antibonding character by $\sigma^{*\prime}$. The 14e, $3b_2$, $8b_1$, 15e, and 16e orbitals are mainly composed of CO $2\pi^*$ orbitals. Some have a considerable admixture of metal 3d character, such as the $3b_2$, and 15e which may be classified as the antibonding counterparts ("t_{2g}*") of the occupied bonding t_{2g}-like orbitals.

In the occupied spectrum we have above the Cl-p_σ ($21a_1$) the metal−carbonyl π bonding t_{2g}-like 3d orbitals and the Cl

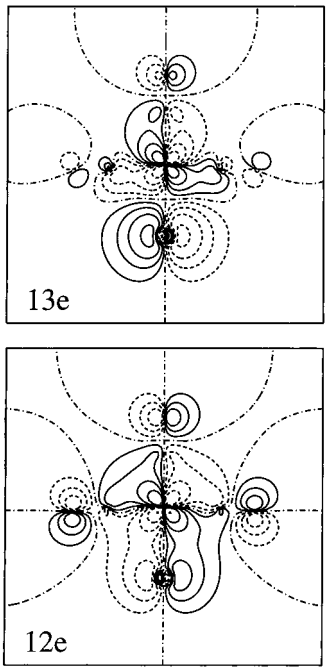

Figure 4. Contour plot of the 12e and 13e orbitals in the *xz*-plane. Contours: see caption to Figure 3.

p_π orbitals. The 12e is the π bonding and the 13e the π antibonding combination of $3d_\pi$ and Cl p_π orbitals (see Figure 4), while the $2b_2$ (d_{xy}) remains a purely $3d_\pi-2\pi^*$ bonding orbital. Note that the $2b_2$ and 12e remain almost degenerate, the loss of one $2\pi^*$ bonding interaction in 12e apparently being compensated by the Cl $3p_\pi$ bonding, but the antibonding with Cl $3p_\pi$ pushes the 13e up so that it becomes more than 1.5 eV higher than its t_{2g} partners. This gap between the HOMO and lower orbitals will be important for the excitation spectrum.

The 13e has more Cl character than the 12e orbital (74 and 22%, respectively), although the Cl 3p orbital energy of the atom is lower than the $Mn(CO)_5$ "t_{2g}"−d_π orbital energy. This can be explained by taking the charges on the atoms into account. Since the chlorine atom bears a charge of approximately −0.4e, its orbital energies are all shifted upward, whereas the $Mn(CO)_5$ orbital energies are shifted downward because of the positive charge on this fragment. This has been taken into account in the qualitative orbital interaction diagram of Figure 2, by positioning the $Mn(CO)_5$ d_π orbital below the Cl 3p orbital so that the $MnCl(CO)_5$ 12e orbital will have more metal character, whereas the 13e orbital has more chlorine character. We wish to caution, however, that the relative Mn $3d_\pi$ and Cl $3p_\pi$ character of the 12e and 13e orbitals is susceptible to considerable change upon removing an electron out of these orbitals by ionization or excitation. We find orbital relaxation in such ionized or excited states to strongly increase the metal character of the 13e. These effects are not peculiar to DFT calculations. Recent CASSCF/CASPT2 caculations by Wilms and Daniel[37] show more pronounced Mn 3d character of 13e already in the ground state and predominant 3d character of the 13e in the first excited state.

Excited States. The 13e HOMO lies 1.5 eV above the other occupied orbitals, and excitations from this orbital to the lowest virtual orbitals are, therefore, of particular interest. Also the lowest excitations from the $2b_2$ and the 12e have been calculated. Higher excitations than the $2b_2 \rightarrow 23a_1$ and $12e \rightarrow 23a_1$ have not been calculated, since those would be too high in energy to play an important role in the photochemistry of $MnCl(CO)_5$.

(37) Wilms, M. P.; Daniel, C. Private communication.

Table 2. Energies (cm^{-1}) and Intensities for Electronic Transitions in $MnCl(CO)_5$

state	transition	character	type	energy (cm^{-1})	intensity	exptl bands[a]
a^3E	$13e \rightarrow 22a_1$	MnCl $\pi^* \rightarrow$ MnCl σ^*	Mn/Cl LF	21 207		
a^1E	$13e \rightarrow 22a_1$	MnCl $\pi^* \rightarrow$ MnCl σ^*	Mn/Cl LF	23 604[b]	0.083 1	26 520
b^3E	$13e \rightarrow 7b_1$	MnCl $\pi^* \rightarrow d_{x^2-y^2}$	Mn/CO LF	29 118		
a^3A_1	$13e \rightarrow 14e$	MnCl $\pi^* \rightarrow 2\pi^*$	Mn,Cl $\rightarrow$ CO CT	30 020		
a^1A_1	$13e \rightarrow 14e$	MnCl $\pi^* \rightarrow 2\pi^*$	Mn,Cl $\rightarrow$ CO CT	30 539[b]	0.139	
c^3E	$13e \rightarrow 3b_2$	MnCl $\pi^* \rightarrow 2\pi^*$	Mn,Cl $\rightarrow$ CO CT	30 861		
d^3E	$13e \rightarrow 8b_1$	MnCl $\pi^* \rightarrow 2\pi^*$	Mn,Cl $\rightarrow$ CO CT	30 936		
b^1E	$13e \rightarrow 7b_1$	MnCl $\pi^* \rightarrow d_{x^2-y^2}$	Mn/CO LF	32 138[b]	0.000 201	
c^1E	$13e \rightarrow 3b_2$	MnCl $\pi^* \rightarrow 2\pi^*$	Mn,Cl $\rightarrow$ CO CT	33 022[b]	0.000 371	
a^3B_2	$2b_2 \rightarrow 22a_1$	$d_{xy} \rightarrow$ MnCl σ^*	Mn/Cl LF	33 077		
d^1E	$13e \rightarrow 8b_1$	MnCl $\pi^* \rightarrow 2\pi^*$	Mn,Cl $\rightarrow$ CO CT	34 226[b]	0.107	
e^3E	$12e \rightarrow 22a_1$	MnCl $\pi \rightarrow$ MnCl σ^*	Mn/Cl LF	34 584		
a^3A_2	$2b_2 \rightarrow 7b_1$	$d_{xy} \rightarrow d_{x^2-y^2}$	Mn/CO LF	34 749		
a^1B_2	$2b_2 \rightarrow 22a_1$	$d_{xy} \rightarrow$ MnCl σ^*	Mn,Cl LF	34 834		
e^1E	$13e \rightarrow 23a_1$	MnCl $\pi^* \rightarrow MnCO_{ax}$ σ^*	Mn/CO LF	35 011[b]	0.005 25	
f^3E	$13e \rightarrow 23a_1$	MnCl $\pi^* \rightarrow MnCO_{ax}$ σ^*	Mn/CO LF	35 034		
f^1E	$12e \rightarrow 22a_1$	MnCl $\pi \rightarrow$ MnCl σ^*	Mn/Cl LF	35 995[b]	0.892	37 000
g^3E	$2b_2 \rightarrow 14e$	$d_{xy} \rightarrow 2\pi^*$	Mn $\rightarrow$ CO CT	37 820		
a^1A_2	$2b_2 \rightarrow 7b_1$	$d_{xy} \rightarrow d_{x^2-y^2}$	Mn/CO LF	38 376		
g^1E	$2b_2 \rightarrow 14e$	$d_{xy} \rightarrow 2\pi^*$	Mn $\rightarrow$ CO CT	39 148[b]	2.49	
b^3A_1	$21a_1 \rightarrow 22a_1$	MnCl $\sigma \rightarrow$ MnCl σ^*	Mn/Cl LF	39 549		
b^1A_1	$21a_1 \rightarrow 22a_1$	MnCl $\sigma \rightarrow$ MnCl σ^*	Mn/Cl LF	43 745[b]	2.74	43 000

[a] Reference 18. [b] Symmetry allowed.

Transition intensities were estimated with the program Dipole.[38] The total transition dipole moment was approximated by the transition dipole moment between the initial and final MO.

The results are shown in Table 2.

As expected the two lowest excited states are the triplet and singlet states corresponding to the $13e \rightarrow 22a_1$ (Mn−Cl $\pi^* \rightarrow$ Mn−Cl σ^*) transition. These states are calculated at 21 207 and 23 604 cm^{-1}, respectively. As mentioned earlier, the character of both the 12e and 13e orbitals changes upon excitation from the 13e orbital. In the excited state, the 12e acquires more Cl 3p character, while the Mn $d_{xz/yz}$ character of the 13e orbital increases. The calculated transition energies are in reasonable agreement with the first broad band in the experimental spectrum. The character of the first transition is beyond doubt, although the different ways it has been denoted may reflect genuine differences of opinion rather than being just a matter of semantics. In the past it has always been designated as a d $\rightarrow$ d ($d_\pi \rightarrow d_{z^2}$) or LF transition. This, however, should not carry the implication—as it sometimes did—of antibonding Mn−CO_{ax} character and therefore expected photoactivity with respect to axial CO dissociation. Our present results and the orbital composition of Pierloot *et al.*[4,5] indicate that the Mn−Cl $\pi^* \rightarrow$ Mn−Cl σ^* transition, or the Mn/Cl LF transition, is a more appropriate description. This has also been suggested by McLean.[19] It is not a Mn/CO LF transition. This difference in character, from what has been generally assumed, sheds some doubt on the assumption of Mn−CO_{ax} dissociative character. This point will be addressed in the next section.

The $22a_1$ lies about 1 eV below the other virtual orbitals, and excitations to those higher virtuals come at energies that are some 8000 cm^{-1} higher than the $13e \rightarrow 22a_1$ transition. Because of the near degeneracy of the 14e, $7b_1$, $3b_2$, $8b_1$, $23a_1$, and 15e orbitals, many excitations out of the 13e to this set of virtuals are present between 29 000 and 35 000 cm^{-1}, of which all transitions to singlet states are allowed. The first transition with Mn/CO LF character, the 13e to $7b_1$ ($d_{x^2-y^2}$), occurs at 29 118 cm^{-1} and 32 138 cm^{-1} for triplet and singlet, respectively. This LF transition has the expectd low intensity, but this excited state is interesting in view of its probably strongly Mn−CO_{eq} dissociative character. At similar energy, at 30 020 and 30 539 cm^{-1}, the first charge transfer (CT) excitations occur, corresponding to the singlet and triplet $13e \rightarrow 14e$ transitions. They have Mn,Cl $\rightarrow$ CO $2\pi^*$ CT character and much higher intensity. Although an e $\rightarrow$ e transition gives rise to A_1, A_2, B_1, and B_2 states, only the mean energy of these states has been calculated, since no major differences between these four states are expected. As seen from the intensities in Table 2, the $13e \rightarrow 14e$ transition may contribute to the high-energy side of the first band, which may partly account for its broadness. The lowest Mn/CO_{ax} LF transitions, the $13e \rightarrow 23a_1$, Mn−Cl $\pi^* \rightarrow$ Mn−CO_{ax} σ^* triplet and singlet states, have been calculated at 35 034 and 35 011 cm^{-1}, respectively. They have low intensity, as was the case for the Mn/CO_{eq} LF transitions, but are photochemically very interesting since, according to the results for $Mn_2(CO)_{10}$,[3b] these states are expected to be strongly Mn−CO_{ax} dissociative.

Until ca. 35 000 cm^{-1} we encounter most of the excitations out of 13e into the $22a_1$−15e set of virtuals (which have all been calculated except the ones into 15e), but above this energy transitions out of the $2b_2$, 12e, and $21a_1$ start to play a role. At 33 077 cm^{-1} the first transition arising out of the HOMO-1 orbital, to the $^3B_2(2b_2(d_{xy}) \rightarrow 22a_1(\sigma^*))$ triplet excited state, is found, its singlet component being located at 34 834 cm^{-1} (the $A_1 \rightarrow B_2$ transition is forbidden). The $12e \rightarrow 22a_1$ (σ^*) excitations are very close. The intensity is surprisingly large, and these transitions will contribute to the band around 37 000 cm^{-1}, although the $2b_2 \rightarrow 14e$ transition at 39 148 cm^{-1} has high intensity and will contribute most. This is a genuine CT transition, which can account for the strong solvatochromic behavior[17] of the corresponding band.

The $2b_2$ (d_{xy}) $\rightarrow$ $7b_1$ ($d_{x^2-y^2}$) Mn/CO LF transition, which may be expected to be Mn−CO_{eq} dissociative, is calculated in this region, at 38 376 cm^{-1} (singlet; the triplet is at 34 749 cm^{-1}). This transition is forbidden.

The only interesting transition from the point of view of Mn−Cl bond breaking is the Mn−Cl $\sigma \rightarrow \sigma^*$, $21a_1 \rightarrow 22a_1$ excitation. The triplet and singlet states corresponding to this transition are located at 39 549 and 43 745 cm^{-1}, respectively. They will contribute to the high-energy band at 43 000 cm^{-1}, but other transitions which were not calculated here, will also contribute to this band.

(38) Wilms, M. P. Internal report; Free University: Amsterdam, 1995.

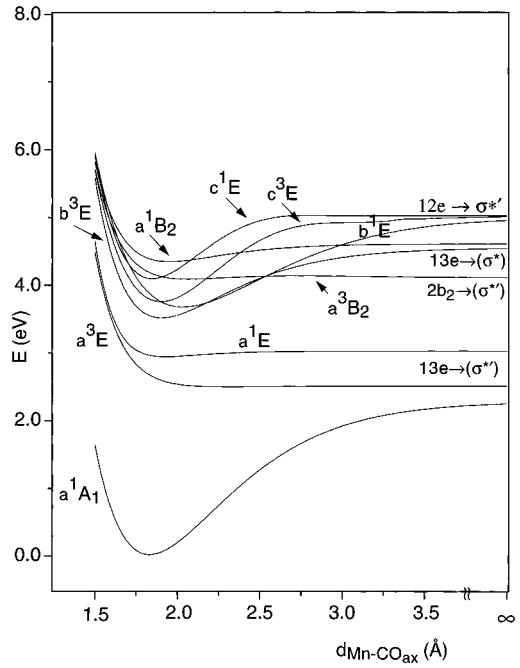

Figure 5. Potential Energy Curves for the dissociation of axial CO in $MnCl(CO)_5$.

4. Photochemistry

Potential Energy Curves for Axial CO Loss. For the ground and lowest excited states we have calculated PECs for loss of the axial CO ligand. The a−c^{1,3}E curves are shown in Figure 5. Of all the curves above the c^{3}E we have, apart from the "companion" c^{1}E, only drawn a^{1,3}B$_2$, since these are the only dissociative ones. The a^{1,3}B$_2$ curves around R_e in fact cross many PECs of other symmetries (not shown in the figure, but see the excitation energies at R_e in Table 2), which, however, all have bonding shapes similar to c^{1,3}E. That these higher excited states (except for the a^{1,3}B$_2$) do not readily lead to CO dissociation may be judged already from the behavior of the relevant orbital energies as a function of Mn−CO distance (see discussion below). Their energies are too high anyway to be populated by the UV−vis excitation used in the photochemical experiments.

The calculated PEC for the ground state has a shallow minimum, which agrees well with the rather low IR frequency for Mn−C vibrations. The asymptotic dissociation limit lies at 2.31 eV above the equilibrium energy, corresponding to a dissociation energy of 222 kJ/mol. This is near the DFT value of 200 kJ/mol for $Mn_2(CO)_{10}$.[3b] Restricted Hartree−Fock calculations by Davy and Hall lead, as usual in the case of a metal−carbonyl bond, to a much lower dissociation energy of 86.9 kJ/mol.[10] When relaxation effects are included, our calculated dissociation energy drops to 176 kJ/mol and the CO's bend toward the Cl, because of the bonding overlap between these fragments. No experimental dissociation energies are known since thermal loss of an equatorial CO is more favorable (*vide infra*).

Before discussing the excited state PECs, it is instructive to consider the orbital characters and energies in the ground state at various Mn−CO_{ax} distances (Figure 6). The most remarkable feature in Figure 6 is the steep descent of the Mn−CO_{ax} σ antibonding 23a$_1$ orbital (it is accompanied by a rise of the σ bonding 20a$_1$ orbital, not shown in the figure), whereas the other orbitals are relatively little affected. As a result the 23a$_1$ (σ*′) orbital very soon crosses the Mn−Cl σ antibonding orbital 22a$_1$ (σ*), already near a Mn−CO_{ax} distance of 2 Å.

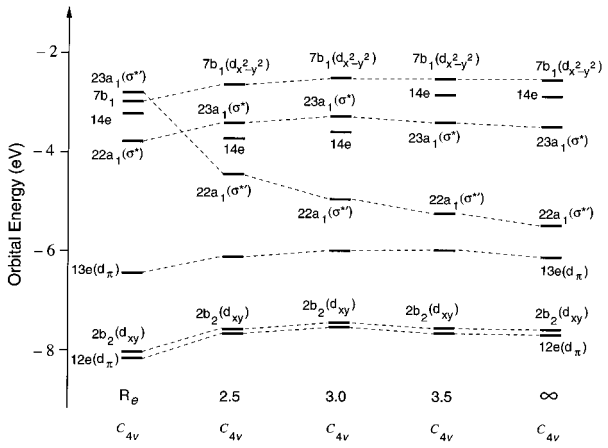

Figure 6. Orbital energies and dominant characters of the highest occupied and lowest unoccupied MO's at several Mn−CO_{ax} bond lenghts.

The lowest excited states of E symmetry, a^{1}E and a^{3}E, will have 13e π* → 22a$_1$ σ* character before the crossing point, but change to 13e π* → 23a$_1$ σ*′ in the crossing region. Since the 13e π* → 22a$_1$ σ* excitation does not affect the Mn−CO_{ax} bond, we would expect the a^{1}E and a^{3}E PECs to be bonding, i.e., exhibit a minimum close to the equilibrium distance and curve upward at longer distances. A barrier would then indicate the avoided crossing to the descending PEC of the excited state with 13e π* → 23a$_1$ σ*′ character, which is asymptotically calculated to lie at much lower energy than the 13e π* → 22a$_1$ σ*(Mn−Cl) state (cf. Figures 5 and 6). We note, however, that the singlet a^{1}E PEC in Figure 5 has only a very weak minimum, and the triplet a^{3}E none at all. The lack of a barrier can be understood from the very rapid lowering of the 23a$_1$ (σ*′) orbital with Mn−CO_{ax} distance, which leads to very rapid descent of the initially high-lying 13e → 23a$_1$ (σ*′) state. This leaves the a^{1,3}E PECs hardly any room to curve upward, and apparently a sufficiently large interaction between the states exists to make the crossing strongly avoided and virtually suppresses any barrier. Exactly the same situation has been observed for axial CO dissociation in $Mn_2(CO)_{10}$.[3b] Of course, the 13e → 23a$_1$ (σ*′) states, which are the e^{1}E, f^{3}E states at equilibrium geometry, cross with the lower ^{1,3}E states before becoming the lowest one. This means that 13e → σ*′ character shows up in successively lower E states before ending up in the lowest one, the a^{1,3}E.

The next higher E PECs are bonding, since no Mn−CO_{ax} antibonding orbital is occupied in these states. The first correspond at R_e to excitations to d$_{x^2-y^2}$ (b^{1,3}E) or 2π* (c and d^{1,3}E). It is clear from Figure 6 that asymptotically, at large Mn−CO_{ax} distance, the first excited states above the low-lying 13e → σ*′ will be 13e → σ* and 12e → σ*′. So b^{1,3}E and c^{1,3}E will asymptotically hold this character. This implies that the electronic character of these states changes during CO_{ax} dissociation, first to 13e → σ*′ character when this excitation "on its way down" crosses these excited states, and next to their asymptotic nature. As a consequence these PECs do not exhibit such a deep well as the ground state PEC but are more shallow. The b^{1,3}E states, which have 13e → 7b$_1$ (d$_{x^2-y^2}$) character at R_e (see Table 2), asymptotically hold the 13e → σ* character that the a^{1,3}E had at R_e. The c^{1,3}E states become asymptotically 12e → σ*′ excited states. The excitation out of the 12e orbital leads to considerable orbital relaxation, asymptotically even more so than at R_e. As a result 12e virtually loses all 3d character, which explains the small singlet−triplet splitting of the asymptotic c^{1}E and c^{3}E curves. The avoided crossing to the 12e → σ*′ excited state does not make the c^{1,3}E PECs dissociative, the asymptotic

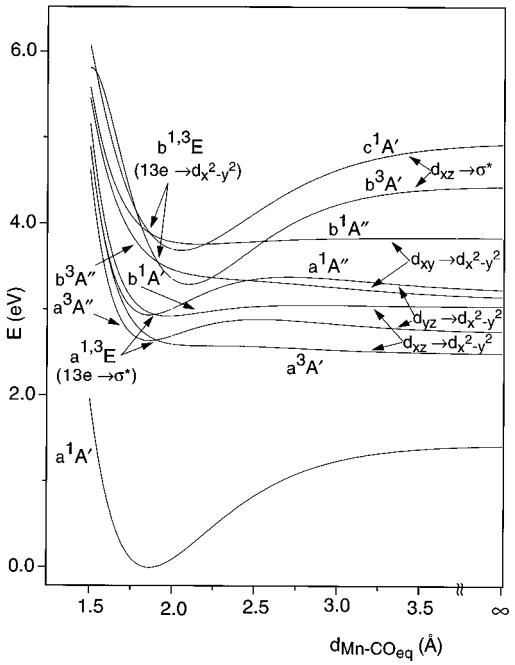

Figure 7. Potential energy curves for the dissociation of equatorial CO in $MnCl(CO)_5$.

energy is still 0.9−1.25 eV above the energy at equilibrium distance. The avoided crossing, however, clearly shows up in the flat behavior of the $c^{1,3}E$ PECs at larger distances.

We have drawn in Figure 5 one set of PECs for another symmetry, namely, the pair of dissociative states a^3B_2 and a^1B_2 states that correspond at equilibrium geometry to excitation from the second highest occupied molecular orbital to the Mn−Cl σ^* orbital, i.e., the $2b_2 \rightarrow 22a_1$, $d_{xy} \rightarrow$ Mn−Cl σ^* transition. As in the case of the $a^{1,3}E$ $13e \rightarrow 22a_1$ excited state, the dissociative behavior is brought about by a change of character, again due to the rapid descent of the $\sigma^{*\prime}$ orbital. The $a^{1,3}B_2$ states correspond asymptotically to the $d_{xy} \rightarrow Mn-CO_{ax}$ $\sigma^{*\prime}$ transition. The a^3B_2 and a^1B_2 states mirror, at a higher energy, the behavior of the a^3E and a^1E states since they correspond to excitations out of $2b_2$ rather than 13e but are otherwise analogous. They are very slightly bonding for the singlet state and dissociative for the triplet state. We have chosen to present this behavior in the figure, although strictly speaking the avoided crossing of these B_2 curves with the B_2 states arising from the lower lying (at R_e) $13e \rightarrow 14e$ should be taken into account. The "diabatic" $a^{1,3}B_2$ PECs in the figure are, however, interesting for the photochemistry upon higher energy excitation; see below.

Potential Energy Curves for Equatorial CO Loss. For equatorial CO loss excitations from the 13e HOMO to the three lowest virtual orbitals at equilibrium geometry and the $2b_2 \rightarrow 22a_1$ transition are investigated. The PECs for the states that correspond at equilibrium geometry to $a^{1,3}E$ ($13e \rightarrow$ Mn−Cl σ^*) and $b^{1,3}E$ ($13e \rightarrow d_{x^2-y^2}$) are displayed in Figure 7. The set of $13e \rightarrow$ CO $2\pi^*$ Mn,Cl → CO CT transitions ($a^{1,3}A_1$, $c^{1,3}E$, $d^{1,3}E$, see Table 2) have been omitted from the figure.

Again the minimum in the ground state PEC is rather shallow in accord with the low frequencies of the Mn−C vibrations. The asymptopic dissociation limit lies at 1.43 eV, which corresponds to a dissociation energy of 138 kJ/mol. When relaxation effects are included, the dissociation energy drops to 99 kJ/mol, in reasonable agreement with the experimental value of 115 kJ/mol.[39] Davy and Hall report a restricted Hartree−Fock (RHF) dissociation energy of 77 kJ/mol.[10]

(39) Angelici, R. J.; Basolo, F. *J. Am. Chem. Soc.* **1962**, *84*, 2495.

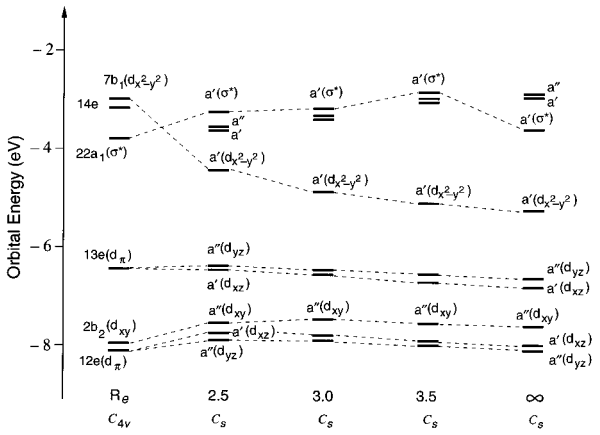

Figure 8. Orbital energies and dominant characters of the highest occupied and lowest unoccupied MO's at several Mn−CO_{eq} bond lengths.

Before discussing the nature of the excited state PECs, we focus on the behavior of the orbitals during the release of CO. The orbital energies at several Mn−CO_{eq} distances are shown in Figure 8 together with their predominant character. As in the case of axial CO loss, the energy of the Mn−CO σ antibonding orbital, in this case the $7b_1$ $d_{x^2-y^2}$ orbital, decreases very rapidly upon elongating the Mn−CO distance. It crosses the $22a_1$ Mn−Cl σ^* orbital at approximately 2.2 Å, which crossing will be avoided since both the B_1 and A_1 symmetries in C_{4v} change to A′ in the C_s point group symmetry that holds upon Mn−CO_{eq} bond elongation. As a result the a′ LUMO changes character from Mn−Cl σ^* to "$d_{x^2-y^2}$" (Mn−CO_{eq} σ antibonding) after the crossing. The lowest excited states in the CO-loss product will clearly be the excitations from the three highest occupied orbitals to the $d_{x^2-y^2}$ LUMO, as indeed indicated in Figure 7. Note that the 13e orbitals, which are degenerate in C_{4v} symmetry, split into an a′ ("d_{xz}") and an a″ ("d_{yz}") orbital, assuming the leaving CO to be the one along the *x*-axis (and Cl along the *z*-axis). For notational convenience we denote these orbitals as d_{xz} and d_{yz}, also in Figures 7 and 8, but of course we should keep in mind that these Mn−Cl d_π−p_π antibonding orbitals have in the ground state actually more Cl p_π character, while the 12e derived pair has more d_π character (however, considerable changes in the relative Cl and Mn contributions occur upon excitation; see above).

The PECs of the lowest A′ and A″ states, arising from the $a^{1,3}E$ states, show a similar dissociative behavior (at least the A′ components) as the lowest E states for the dissociation of an axial CO. The situation is indeed very similar: the dissociative states arising from $13e \rightarrow 7b_1$ ($d_{x^2-y^2}$) excitations, which are at R_e some 8000−9000 cm^{-1} higher than the lowest excited states of E symmetry, rapidly cross upon Mn−CO_{eq} bond lengthening with the states located below them, and the A′ and A″ states resulting from the lowest E states ($a^{1,3}E$) rapidly change character from $13e \rightarrow 22a_1$ Mn−Cl σ^* at equilibrium geometry to $13e \rightarrow d_{x^2-y^2}$ Mn−CO_{eq} $\sigma^{*\prime}$ character at larger Mn−CO_{eq} distances.[41] The crossing is so soon that these A′ and A″ states are either weakly bonding or dissociative. The difference in behavior of the A′ and A″ states is striking. The A′ states are purely (a^3A') or nearly (b^1A') dissociative, whereas the a^1A'' and a^3A'' states still exhibit a clear bonding minimum. This difference can be explained if one takes into account the

(40) (a) Atwood, J. D.; Brown, T. L. *J. Am. Chem. Soc.* **1975**, *97*, 3380. (b) Atwood, J. D.; Brown, T. L. *J. Am. Chem. Soc.* **1976**, *98*, 3155. (c) Atwood, J. D.; Brown, T. L. *J. Am. Chem. Soc.* **1976**, *98*, 3160.

(41) For reasons of clarity orbitals in C_s symmetry are designated by their symmetry label in the C_{4v} ground state equilibrium geometry.

different nature of the a′ and a″ orbitals, which form the 13e orbitals at equilibrium geometry. The a′ orbital contains, apart from the Cl p_π, the d_π orbital (d_{xz}) with lobes directed toward the leaving CO (along the *x*-axis), whereas the a″ orbital contains the d_π orbital (d_{yz}) orthogonal to this Mn−CO_{eq} axis. If the CO is complety dissociated, the a′ orbital has an interaction with only one equatorial CO, whereas the a″ orbital interacts with two equatorial CO's. After excitation out of the 13e orbital, CO loss will preferably occur in such a way that at the dissociation limit the a″ component of the 13e orbital is fully occupied, while the a′ orbital is singly occupied, i.e., in the A′ state. This preference is reflected in the more strongly dissociative behavior of the a^3A', b^1A' PECs compared to the a^3A'', a^1A'' PECs. Note that this electronic structure argument would at the one-electron level lead one to expect the a′ ("d_{xz}") to lie above the a″ ("d_{yz}"), but this is not the case (see Figure 8). The breakdown of this simple one-electron picture is related to the predominantly Cl p_π character of the 13e in the ground state and the orbital relaxations accompanying ionization and excitation out of this orbital mentioned earlier. Note that the 12e derived a′ and a″ orbitals, which are the bonding combinations of Mn $3d_\pi$ with Cl $3p_\pi$, do exhibit the expected ordering (see Figure 8).

The PECs that arise from the $b^{1,3}E$ states show just the opposite behavior in that now the A″ states (b^1A'' and b^3A'') are dissociative, while the A′ states (c^1A' and b^3A') are unambiguously bonding. The reason is that the A″ states can asymptotically become $d_{xy} \rightarrow d_{x^2-y^2}$ excited states, whereas the A′ states cannot asymptotically become excited states to the descending $d_{x^2-y^2}$ orbital (cf. the orbital energy pattern in Figure 8). Note that the change of electronic character along the b^1A'' and b^3A'' PECs is now due to a change in the orbital out of which the excitation takes place, namely, from the 13e component d_{yz} to the lower lying $2b_2(d_{xy})$. The excitation is to the descending $d_{x^2-y^2}$ all along these PECs, which are dissociative but would even be more strongly dissociative had not the $13e(d_{yz}) \rightarrow d_{x^2-y^2}$ character changed to the higher excitation $2b_2(d_{xy}) \rightarrow d_{x^2-y^2}$. The $d_{yz} \rightarrow d_{x^2-y^2}$ character descends down into the $a^{1,3}A''$ (*vide supra*). Concerning the A′ components of the $b^{1,3}E$, we note that the $d_{xz} \rightarrow d_{x^2-y^2}$ character that they have at R_e has already been observed to revert to the lowest lying A′'s (a^3A', b^1A'). The $b^{1,3}E(A')$ become asymptotically 13e("d_{xz}") $\rightarrow \sigma^*$(Mn−Cl), which excitation is asymptotically somewhat lower than the 12e-a′$(d_{xz}) \rightarrow d_{x^2-y^2}\ \sigma^{*\prime}$. The corresponding PECs have a similar bonding behaviour for equatorial CO loss as the ground state PEC since the $d_{xz} \rightarrow d_{x^2-y^2}$ excited state from which this PEC starts out at R_e is not so much higher in energy than the $d_{xz} \rightarrow \sigma^*$(Mn−Cl) excitation that it becomes asymptotically.

Comparing the equatorial CO dissociation to the axial CO dissociation, we note that we have, for both axial and equatorial CO loss, dissociative states that correspond asymptotically to excitations out of the 13e ("d_{xz},d_{yz}") and the $2b_2(d_{xy})$ to the descending orbitals, $d_{z^2}\ \sigma^{*\prime}$ in the case of axial CO and $d_{x^2-y^2}\ \sigma^{*\prime}$ in the case of equatorial CO. In both cases the lowest excited $a^{1,3}E$ states are dissociative, becoming asymptotically $13e(d_{xz},d_{yz}) \rightarrow d_{z^2}\ \sigma^{*\prime}$ and 13e−a′$(d_{xz}) \rightarrow d_{x^2-y^2}\ \sigma^{*\prime}$ excited states, respectively. The important difference is that in the case of equatorial CO also the relatively low-lying $b^{1,3}E$ excited states, which are just accessible in the photochemical experiments, are dissociative, leading asymptotically to $d_{xy} \rightarrow d_{x^2-y^2}\ \sigma^{*\prime}$ states, whereas in the case of axial CO the $b^{1,3}E$ excited states are bonding. In the case of axial CO only the higher lying $a^{1,3}B_2$ states, leading to $d_{xy} \rightarrow d_{z^2}\ \sigma^{*\prime}$ states asymptotically, are dissociative. These states are at too high energy to play a role in the photochemical experiments, and axial CO dissociation is therefore expected to be less efficient. As a matter of fact the excitation to b^1E, although it may be just accessible, has quite low intensity (see Table 2). It may therefore be the much higher intensity excitation to a^1A_1, followed by intersystem crossing to b^3E and ensuing dissociation of equatorial CO, that provides the mechanism for the increase of the quantum yield at higher excitation energy.

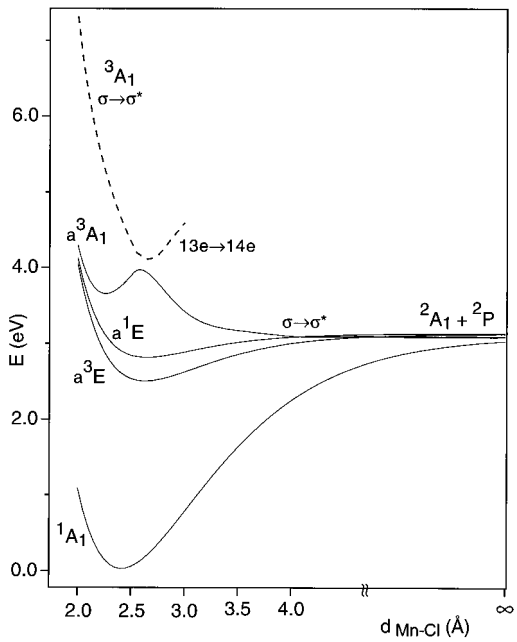

Figure 9. Potential energy curves for Mn−Cl bond homolysis. The avoided crossing between to two $^3A_1$ states is not calculated accurately and is only indicated.

Potential Energy Curves for Mn−Cl Homolysis. Since no Mn−Cl heterolysis or homolysis is experimentally observed, only a few PECs along the Mn−Cl axis have been calculated. According to the calculations the first excited ^2E state of $Mn(CO)_5^\bullet$ lies 1.86 eV above its ground state.[3b] The states of $MnCl(CO)_5$ correlating with this ^2E state will thus not play a role in the photochemistry of $MnCl(CO)_5$, since they can only be reached with far-UV light. Heterolysis, although feasible in solution, is not taken into account since the energies of the ions in the gas phase are rather high. The radicals are calculated to be about 4 eV (i.e., about 400 kJ/mol) more stable than $Mn(CO)_5^+$ and Cl^- in the gas phase. Therefore only the PECs of the $^{1,3}E$ and $^{1,3}A_1$ states, which asymptotically correspond to the $^2A_1 + {}^2P$ ground states of $Mn(CO)_5^\bullet$ and $Cl^\bullet$, have been calculated.

The lowest state that correlates with the asymptotic $^2A_1 + {}^2P$ fragment ground states is the $^1A_1$ ground state. The PEC of this state shows that Mn−Cl homolysis requires much more energy than CO dissociation, i.e., 297 kJ/mol. When relaxation effects are included, the homolysis energy becomes 268 kJ/mol, in excellent agreement with the experimental value of 268 kJ/mol.[42]

The lowest ^3E and ^1E states, corresponding to the Mn−Cl $\pi^* \rightarrow$ Mn−Cl σ^*, $13e \rightarrow 22a_1$ excitation, directly correlate with the ground state of the radicals $Mn(CO)_5^\bullet$ and $Cl^\bullet$. As can be seen from Figure 9 excitation into these states does not supply enough energy to homolytically break the Mn−Cl bond. Therefore Mn−Cl bond homolysis cannot occur even though the lowest excited states do correlate with the lowest states of

(42) Connor, J. A. *Organometallics* **1982**, *1*, 1166.

the radicals. The absence of Mn−Cl homolysis is therefore attributed to the high thermodynamic stability of the Mn−Cl bond.

The $^3A_1$ state correlating with the $^2A_1 + {}^2P$ ground state of the radicals corresponds from ca. 2.7 Å onward to the Mn−Cl $\sigma \rightarrow$ Mn−Cl σ^* $21a_1 \rightarrow 22a_1$ transition. The orbital energies (not shown here) show the expected behavior of, on the one hand, rapid lowering of the Mn−Cl σ^* $22a_1$ LUMO, which without crossings becomes asymptotically the singly occupied σ_{hy} hybrid of the $Mn(CO)_5^\bullet$ radical, and, on the other hand, an increase in energy of the Mn−Cl σ $21a_1$, which asymptotically becomes the $Cl^\bullet$ $3p_\sigma$ atomic orbital. The diminishing gap between these orbitals corresponds to the dissociative character of the a^3A_1 PEC in the asymptotic tail.

At the equilibrium geometry the lowest $^3A_1$ state, arising from the 13e → 14e transition, has a lower energy than the $\sigma \rightarrow \sigma^*$ state and an avoided crossing between these two states will thus occur. Therefore, the PEC of the 13e → 14e triplet state has also been calculated near equilibrium geometry. The barrier resulting from the avoided crossing is clearly visible on the a^3A_1 PEC in Figure 9. The $\sigma \rightarrow \sigma^*$ excitation energy has been calculated at shorter distances than 2.7 Å, and a sketch of the steeply descending $\sigma \rightarrow \sigma^*$ state is given in Figure 9, without however trying to map out in detail the avoided crossings through which the $\sigma \rightarrow \sigma^*$ character descends (except for the last one). Excitation to the b^1A_1,a^3A_1 (13e → 14e) at R_e or to nearby higher excited states can only yield the radical products after crossing the barrier in the a^3A_1 PEC. In this region, many states are present (not drawn in Figure 9) and internal conversion toward lower states will probably be rather fast. As a consequence Mn−Cl bond homolysis is unlikely. It is in fact not even observed with high-energy radiation.[7]

Photochemistry of $MnCl(CO)_5$. Irradiation of $MnCl(CO)_5$ with low-energy light results in occupation of the a^1E state. The excited molecules can then either lose axial (*trans-)* or equatorial (*cis-*) CO after overcoming only a small barrier in both directions or undergo intersystem crossing to the a^3E state. From this latter state axial and equatorial CO loss can occur without any barrier. Indeed, photochemical *cis-* and *trans*-CO exchange has been observed in ^{13}CO exchange experiments.[43] It should, however, be cautioned that this does not strictly prove the occurrence of both primary photoprocesses, since fast rearrangements may also occur during these exchange processes. Our results do point to the occurrence of both reactions. In this respect they do not substantiate the assumption that photochemical *trans*-CO dissociation is most likely for this type of complex. This assumption has been generally made, and the absence of *trans*-substituted photoproducts upon irradiation of metal pentacarbonyl halides in the presence of a Lewis base has been attributed[7] to rapid rearrangement of the apical $MnCl(CO)_4$ primary photoproduct resulting from *trans*-CO loss to $MnCl(CO)_4$ with Cl in the basal plane. This point has recently been studied in detail by Pierloot *et al.*[4] and Matsubara *et al.*[8c] The results of these studies are relevant for the present work in that we certainly cannot exclude *trans*-CO loss.

The A″ components of the b^3E and b^1E states, which are located at higher energy, are also dissociative for equatorial CO loss, due to crossing by the $2b_2(d_{xy}) \rightarrow 7b_1(d_{x^2-y^2})$ state (see Figure 7), but not for axial CO (see Figure 5). The presence of these states can account for the increase in quantum yield when going to shorter wavelength excitation. Irradiation at 366 nm (27 322 cm^{-1}, 3.39 eV) results in CO loss with a quantum yield of 0.06, whereas irradiation at 313 nm (31 948 cm^{-1}, 3.96 eV) gives a quantum yield of 0.44. Irradiation at 313 nm results in population of the b^1E and b^3E states, most likely by population of the a^1A_1 which has high intensity, followed by intersystem crossing. The A″ components of $b^{1,3}E$ are dissociative for the equatorial CO. The 313 nm radiation may just not be able to populate the higher lying aB_2 states, which are dissociative for the axial CO. Even if the aB_2 states could be reached, release of CO from these states may have lower probability since nonradiative decay to close-lying excited states is expected to be rather fast because of the large density of states in this region. It is therefore expected that the ratio of equatorial to axial CO loss changes in favor of equatorial CO loss when the wavelength of excitation is shortened.

Comparison of the Photochemistry of $Mn_2(CO)_{10}$, $MnH(CO)_5$, and $MnCl(CO)_5$. In this section we will compare the results from calculations of the PECs of $Mn_2(CO)_{10}$ by Rosa *et al.*,[3] those of $MnH(CO)_5$ by Daniel *et al.*,[2g] and the present results on $MnCl(CO)_5$. These can be taken as prototype for respectively $Mn(CO)_5(M')$ (M′ = $Mn(CO)_5$, $Re(CO)_5$, etc.), $MnR(CO)_5$ (R = H, CH_3), and $MnX(CO)_5$ (X = Cl, Br, I). All of these molecules can be built up by combining $Mn(CO)_5$ and another fragment with a singly occupied orbital. The differences between the molecules must thus stem from differences in these fragments and their interaction with $Mn(CO)_5$.

As shown above, the photochemistry of organometallic compounds is primarily determined by the relative energies of the occupied and virtual orbitals in the ground state *and their dependence on the geometry*. The orbital interaction diagrams for the three compounds are given in Figure 2. [The orbital energies for $MnH(CO)_5$ and $Mn_2(CO)_{10}$ were calculated using the same basis set and functional as those for $MnCl(CO)_5$, in previously optimized geometries.[3,35]] The compounds $MnH(CO)_5$ and $MnCl(CO)_5$ both have the Mn−H/Cl σ bonding orbital, with much H 1s and Cl $3p_\sigma$ character, respectively, located below the occupied Mn 3d orbitals. In the case of $MnH(CO)_5$ the e (d_π) orbitals are the $d_{xz/yz}$ orbitals, in $MnCl(CO)_5$ the e orbitals split into two sets of Mn−Cl π and π^* orbitals. In the case of $Mn_2(CO)_{10}$ the ordering is reversed; here the Mn−Mn σ orbital is the HOMO and the e ($d_{xz/yz}$) orbitals (the e_1 π bonding and e_3 π antibonding sets) are at lower energy.[3a] The relatively high energy of the σ orbital in the case of $Mn_2(CO)_{10}$, when compared to $MnCl(CO)_5$ and $MnH(CO)_5$, is caused by the rather high energy of the $Mn(CO)_5$ σ_{hy} hybrid, when compared with the H 1s and Cl 3p orbitals, and by the relatively weak interaction between the σ_{hy} orbitals.

In the case of $MnCl(CO)_5$ and $Mn_2(CO)_{10}$ the Mn−L (L = Cl or $Mn(CO)_5$) σ^* orbital is the LUMO, whereas the Mn−CO_{ax} and Mn−CO_{eq} $\sigma^{*\prime}$ antibonding orbitals are located at higher energy (we denote the Mn−CO_{ax} and Mn−CO_{eq} σ antibonding orbitals, "d_{z^2}" and "$d_{x^2-y^2}$", respectively, both as $\sigma^{*\prime}$). $MnH(CO)_5$ is special in that the Mn−H σ^* orbital is located at very high energy, considerably above the $\sigma^{*\prime}$ orbitals. The LUMO is in this case a CO $2\pi^*$ orbital. The diagram highlights the remarkably stronger interaction of the $Mn(CO)_5$ σ_{hy} hybrid with H 1s than with another $Mn(CO)_5$ σ_{hy}.

The three complexes show a strikingly similar behavior with respect to CO loss, which in all three cases occurs upon irradiation into the lowest energy band. In all cases the $d_{xz/yz}$ → LUMO excited state is dissociative for axial and equatorial[44] CO loss, but only after an (avoided) crossing of the LUMO with the Mn−CO_{ax} or Mn−CO_{eq} $\sigma^{*\prime}$ orbital, respectively. Whether there is a small barrier or not is not important here. Such a barrier may have a large influence on the quantum yield,

(43) Berry, A.; Brown, T. L. *Inorg. Chem.* **1972**, *11*, 1165.

(44) Daniel *et al.* did not calculate PECs for the loss of equatorial CO. There is, however, no reason to assume a different behavior than $MnCl(CO)_5$.

but it can be overcome by several mechanisms.[45] In the case of $Mn_2(CO)_{10}$ there is also the transition $\sigma \rightarrow \sigma^*$ at approximately the same energy (calculated at slightly lower energy but experimentally assigned to slightly higher energy than the $d_{xz/yz} \rightarrow \sigma^*$). The $\sigma \rightarrow \sigma^*$ excited state of $Mn_2(CO)_{10}$ is, however, not Mn−CO dissociative. Thus, we may conclude that Mn−CO dissociation is very similar in these cases. It has little to do with the nature of the LUMO but is caused by the strongly Mn−CO antibonding nature of the $\sigma^{*\prime}$ orbitals. The rapid descent upon Mn−CO bond lengthening of these orbitals leads to the CO dissociation in the lowest excited state. This feature of the electronic structure is peculiar to the $Mn(CO)_5$ fragment, although the substituent influences the precise position of the dissociative state with respect to the other states.

The Mn−H/Cl/Mn homolysis shows large differences between these molecules, which is caused by the large influence of the substituent on the energy of the important orbitals. In the case of $Mn_2(CO)_{10}$, the $\sigma \rightarrow \sigma^*$ triplet state is part of the lowest energy band and bond homolysis thus occurs very easily, being the primary photoprocess, together with Mn−CO dissociation, upon irradiation into the lowest band. In the case of $MnH(CO)_5$ and $MnCl(CO)_5$ the $\sigma \rightarrow \sigma^*$ transitions are at too high energy to be excited directly in the usual photochemical experiment. At long distances the $^3(\sigma \rightarrow \sigma^*)$ excited state will become much lower in energy, and asymptotically it will go to the ground states of the radical fragments. An avoided crossing will thus eventually occur with the lowest $^3A_1$ state, making the lowest $^3A_1$ PEC dissociative at long distances. However, the lowest $^3A_1$ state at equilibrium geometry, corresponding to the 13e → 14e excitation, is already considerably higher than the $d_{xz/yz} \rightarrow$ LUMO type excited state, which is responsible for the lowest band in the experimental spectrum. Even if irradiation takes place at sufficiently high energy to populate the lowest $^3A_1$, the barrier in the lowest $^3A_1$ PEC, related to the avoided crossing (see Figure 9), will drastically reduce the quantum yield for Mn−H/Cl dissociation.

These results fit in nicely with the experimental observations that a primary photoprocess of all of these complexes is Mn−CO dissociation, with higher quantum yield for higher energy radiation due to increased $Mn-CO_{eq}$ dissociation. In $Mn_2(CO)_{10}$ the Mn−Mn bond homolysis[46] is fully competitive with Mn−CO bond dissociation upon irradiation in the lowest band (1:1), the propensity to Mn−CO bond breaking increasing at higher energy. In $MnH(CO)_5$ and $MnCl(CO)_5$ Mn−H/Cl bond homolysis occurs much less readily. Mn−H bond dissociation only occurs upon irradiation with high energy[47] but in much lower yield than Mn−CO bond dissociation, whereas for $MnCl(CO)_5$ no Mn−Cl bond homolysis has (yet) been found.[7] The difference between these systems with respect to the Mn−Mn/H/Cl homolysis can be understood immediately from the positions of the σ and σ^* molecular orbitals (Figure 2).

5. Conclusions

We have considered both the photochemical Mn−CO dissociation and Mn−L σ bond homolysis in the complexes $Mn(CO)_5L$ with L = Cl, H, and $Mn(CO)_5$.

As for the Mn−L photolysis, which readily occurs for the Mn−Mn bond in $Mn_2(CO)_{10}$, but not for the Mn−Cl and Mn−H bonds in $MnCl(CO)_5$ and $MnH(CO)_5$ respectively, we have been able to explain this behavior on the basis of the relative positions of the σ and σ^* orbitals in the occupied and virtual orbital level spectra.

As for the metal−carbonyl dissociation our calculations point to a mechanism of photochemical CO loss that differs substantially from the generally accepted one, which invokes dissociation occurring upon ligand-field excitation. In the case of $MnCl(CO)_5$ Wrighton *et al.*[7] suggested on the basis of ligand field theory that transitions to the lowest excited state would imply occupation of a d_{z^2}, which would, due to antibonding with axial CO, lead directly to axial CO loss. Higher energy excitation would lead to occupation of the higher $d_{x^2-y^2}$ orbital and result in loss of an equatorial CO. This explanation directly accounts for the increase in quantum yield upon higher energy excitation. A similar explanation of the photochemistry was presented by Pierloot *et al.*[4]

Our calculations, however, demonstrate that the LUMO is not antibonding for either axial or equatorial CO. *The lowest excited state only becomes dissociative for both axial and equatorial CO after avoided crossing with a state which is Mn−CO dissociative but which is at too high energy at R_e to be populated directly*. The high-lying states are the 13e → $23a_1$ (d_{z^2} $\sigma^{*\prime}$) and 13e → $7b_1$ ($d_{x^2-y^2}$ $\sigma^{*\prime}$) LF excited states for axial and equatorial CO loss, respectively. The calculations show that the nature of the LUMO at the equilibrium geometry does not primarily determine the photochemistry of this complex. The geometry dependence of all antibonding orbitals has to be taken into account. This result—which substantiates previous findings for $Mn_2(CO)_{10}$[3b]—implies an important *caveat* for the general practice of trying to interpret photochemical events in transition metal complexes on the basis of molecular orbital diagrams *at the equilibrium geometry*. A very clear example is $Cr(CO)_6$, where we have recently found[48] precisely the same situation to apply: the ligand-field excited states are at R_e at high energy, but they descend so rapidly upon Cr−CO bond lengthening that they very soon cross the lowest excited state, which has CT character at R_e, so that the lowest excited state PEC becomes dissociative. Recent sophisticated CASSCF/CASPT2 calculations of the optical spectrum of $Cr(CO)_6$ by Pierloot *et al.*[49] provide support for this reassessment of the role of LF states in the photochemical metal−carbonyl dissociation process in that they show that the LF excited states of $Cr(CO)_6$ are—contrary to the original assignment by Beach and Gray[50]—located rather high in the spectrum, the photodissociative lowest excited states having clear CT character at R_e.

IC960688+

(45) Schinke, V. *Photodissociation Dynamics*; Cambridge University Press: Cambridge, U.K., 1993.
(46) Kobayashi, T.; Ohtani, H.; Noda, H.; Teratani, S.; Yamazaki, H.; Yasufuku, K. *Organometallics* **1986**, *5*, 110.
(47) (a) Church, S. P.; Poliakoff, M.; Timney, J. A.; Turner, J. J. *J. Am. Chem. Soc.* **1981**, *103*, 7515. (b) Church, S. P.; Poliakoff, M.; Timney, J. A.; Turner, J. J. *Inorg. Chem.* **1983**, *22*, 3259.
(48) Pollak, C.; Baerends, E. J.; Rosa, A. Unpublished results.
(49) Pierloot, K.; Tsokos, E.; Vanquickenborne, L. G. *J. Phys. Chem.*, to be published.
(50) Beach, N. A.; Gray, H. B. *J. Am. Chem. Soc.* **1968**, *90*, 5713.